Water Science & Technology

Water Science & Technology Vol 89 No 5, 1107 doi: 10.2166/wst.2024.054

Hydrothermal-assisted synthesis of Sr-doped SnS nanoflower catalysts for photodegradation of metronidazole antibiotic pollutant in wastewater promoted by natural sunlight irradiation

Tayeb Bouarroudj[a,*], Youcef Messai[b,c], Lamine Aoudjit[d], Beddiaf Zaidi[e], Djamila Zioui[d], Amel Bendjama[f], Samiha Mezrag[g], Abdelmounaim Chetoui[h], Ilyas Belkhettab[h,i] and Khaldoun Bachari[a]

[a] Scientific and Technical Research Center in Physico-Chemical Analyses (CRAPC), Industrial zone, PO-box 384 Bousmail, Tipaza, Algéria
[b] Laboratory for the Study of Surfaces and Interfaces of Solid Matter (LESIMS), Badji Mokhtar University, Annaba 23000, Algeria
[c] Laboratory of Surfaces and Interfaces Studies of Solid Materials (LESIMS), Faculty of Technology, Ferhat Abbas Setif 1 University, Setif 19000, Algeria
[d] Unité de Développement des Équipements Solaires, UDES/Centre de Développement des Energies Renouvelables, CDER, Bou-ismail, W. Tipaza 42415, Algeria
[e] Department of Physics, Faculty of Material Sciences, University of Batna 1, Batna, Algeria
[f] Research center in industrial technologies CRTI, P.O. Boxe 64, Cheraga, Algiers 16014, Algeria
[g] Département et Laboratoire de Métallurgie et Génie des Matériaux, Faculté des Sciences de l'Ingéniorat Université Badji Mokhtar-Annaba, BP 12 Annaba 23000, Algeria
[h] Research Center in Semiconductors Technology for Energetics (CRTSE), 02 Bd Dr Frantz Fanon, 7- Merveilles, Algiers, Algeria
[i] Laboratory of Electrochemistry-Corrosion, Metallurgy and Inorganic Chemistry, Faculty of Chemistry, USTHB, BP32, 16111 Algiers, Algeria
*Corresponding author. E-mail: bouarroudj.tayeb@crapc.dz

ABSTRACT

In this study, we report a facile hydrothermal synthesis of strontium-doped SnS nanoflowers that were used as a catalyst for the degradation of antibiotic molecules in water. The prepared sample was characterized using X-ray diffraction (XRD), scanning electron microscopy (SEM), and ultraviolet–visible absorption spectroscopy (UV–Vis). The photocatalytic ability of the strontium-doped SnS nanoflowers was evaluated by studying the degradation of metronidazole in an aqueous solution under photocatalytic conditions. The degradation study was conducted for a reaction period of 300 min at neutral pH, and it was found that the degradation of metronidazole reached 91%, indicating the excellent photocatalytic performance of the catalyst. The influence of experimental parameters such as catalyst dosage, initial metronidazole concentration, initial reaction pH, and light source nature was optimized with respect to metronidazole degradation over time. The reusability of the strontium-doped SnS nanoflowers catalyst was investigated, and its photocatalytic efficiency remained unchanged even after four cycles of use.

Key words: degradation, metronidazole, photocatalysis, Sr-doped SnS, wastewater

HIGHLIGHTS

- Sr-doped SnS is synthesized by the hydrothermal process.
- Sr-doped SnS nanoflowers were selected to remove dyes from water.
- The removal percentage of Sr-doped SnS could reach 91%.
- The reusability of our catalyst Sr-doped SnS was also explored.

GRAPHICAL ABSTRACT

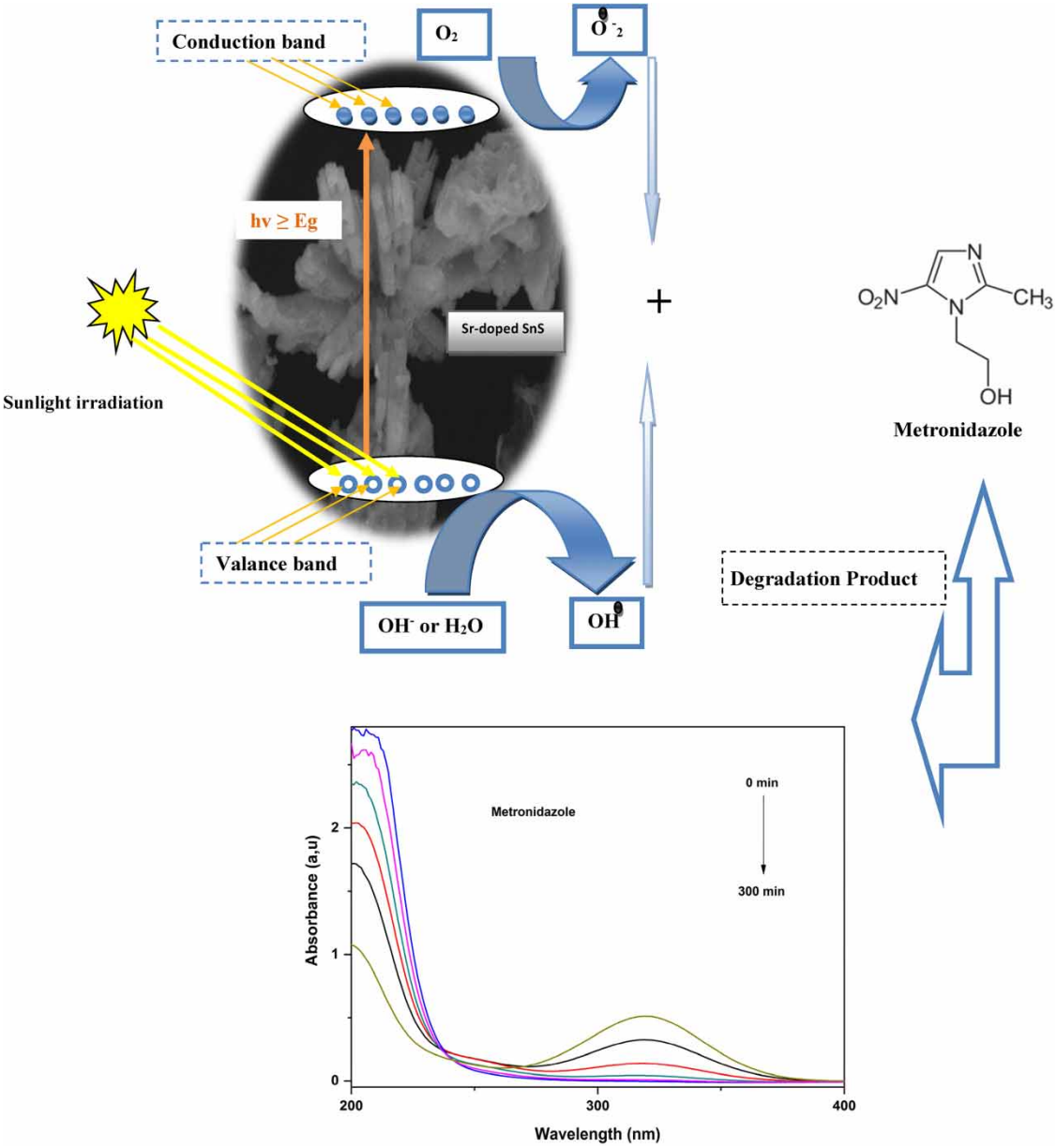

1. INTRODUCTION

Water pollution is a serious environmental problem that occurs when harmful substances, such as chemicals, waste materials, and sewage, contaminate bodies of water like oceans, rivers, and lakes. Human activities such as industrialization, agricultural practices, and improper waste disposal are major contributors to water pollution (Bashir *et al.* 2020; Qadri *et al.* 2020; Akhtar *et al.* 2021; Karri *et al.* 2021; Sarker *et al.* 2021). The consequences of water pollution can be devastating for both aquatic life and humans who rely on these water sources for drinking, irrigation, and recreational purposes. It can lead to the depletion of fish populations, the spread of waterborne diseases, and the contamination of food sources. Addressing water pollution requires a concerted effort from individuals, governments, and industries to adopt sustainable practices and reduce harmful pollutants in our water sources (Weldeslassie *et al.* 2018; Chowdhary *et al.* 2020; Kiliç 2021; Morin-Crini *et al.* 2022).

Water pollution caused by antibiotics, including metronidazole (MNZ), is a growing concern worldwide. When antibiotics are used in human or animal medicine, a portion of the drug is excreted from the body and ends up in wastewater. Treatment plants are not designed to remove antibiotics from wastewater, so they are discharged into rivers, lakes, and oceans. This discharge of antibiotics into water bodies can lead to the development of antibiotic-resistant bacteria, which can pose a serious threat to public health (Polianciuc *et al*. 2020; Baaloudj *et al*. 2021; Jovanovic *et al*. 2021; Tian *et al*. 2021). MNZ, in particular, is an antibiotic used to treat infections such as bacterial vaginosis and periodontitis. It has been found to persist in the environment for long periods and can be toxic to aquatic organisms, even at low concentrations. The accumulation of MNZ in the environment can have detrimental effects on aquatic ecosystems and pose a risk to human health (Bashiri *et al*. 2020; Ighalo *et al*. 2020; Wang *et al*. 2022a; Aoudjit *et al*. 2023).

Eliminating organic pollutants from water is a complex process that requires the use of various techniques. One of the most effective methods is activated carbon filtration, which involves passing water through a bed of activated carbon to remove organic contaminants (Castiglioni *et al*. 2022; Zioui *et al*. 2022; Huang *et al*. 2023; Yang *et al*. 2023). Another technique is reverse osmosis, which uses a semi-permeable membrane to filter out pollutants (Hu *et al*. 2023; Liao *et al*. 2023; Pezeshki *et al*. 2023; Shen *et al*. 2023). Biological treatment, which uses bacteria or other microorganisms to breakdown organic compounds, is also an effective method for eliminating pollutants (Yang *et al*. 2022; Rokkarukala *et al*. 2023; Tian *et al*. 2023). Membrane process represent an efficient, straightforward, and low-cost alternative as a pretreatment step for continuous treatment processes for simultaneous organic and inorganic contaminants' remediation in real industrial effluent sources as reported by Zioui *et al*. (2023). Additionally, advanced oxidation processes (AOPs) such as UV oxidation or ozonation can be used to breakdown organic contaminants into less harmful substances. Overall, a combination of these techniques may be necessary to completely eliminate organic pollutants from water (Liu *et al*. 2022; Li *et al*. 2023; Saoud *et al*. 2023; Wardighi *et al*. 2023). Photocatalysis is a powerful technique used to eliminate organic pollutants from water and air. It involves the use of a catalyst that can convert light energy into chemical energy to breakdown organic molecules into harmless substances such as water and carbon dioxide. This technique is highly effective and environmentally friendly as it does not produce any toxic byproducts or require any additional chemicals. Photocatalysis is becoming an increasingly popular technique of choice for eliminating organic pollutants due to its high efficiency, low cost, and versatility in treating a wide range of contaminants (Sun *et al*. 2023; Yin *et al*. 2023; Yu *et al*. 2023; Wang *et al*. 2023a, 2023b). The decontamination of wastewater (degradation of oil in wastewater) using AOP photocatalysts and solar wastewater treatment (SOWAT) has been reported as possible techniques for wastewater purification using solar radiation for reuse in agriculture and industry (Igoud *et al*. 2019, 2021, 2022; Zioui *et al*. 2019; Martins *et al*. 2021).

Semiconductor photocatalysts, particularly those based on sulfur, have gained significant attention in recent years due to their unique properties and potential applications in various fields. Sulfur-based photocatalysts have a narrow bandgap, allowing them to absorb light in the visible range and generate charge carriers that can facilitate chemical reactions. This property makes them particularly useful in photocatalytic applications, such as environmental remediation, hydrogen production, and organic synthesis. Additionally, sulfur-based photocatalysts are cost-effective and environmentally friendly, making them a promising alternative to traditional photocatalytic materials. Ongoing research in this area aims to optimize the performance of sulfur-based photocatalysts and explore new applications for these versatile materials (Lincho *et al*. 2023; Liu *et al*. 2023; Saoud *et al*. 2023; Zhang *et al*. 2023).

SnS (tin sulfide) is a semiconductor material with a tunable bandgap energy that makes it suitable for various optoelectronic and photovoltaic applications, including photocatalysis. The bandgap energy of SnS ranges from 0.9 to 1.3 eV, which corresponds to the visible to near-infrared light spectrum, making it an efficient absorber of solar radiation. In photocatalysis, SnS-based materials have been used for the degradation of organic pollutants, water splitting, and CO_2 reduction. The unique electronic and optical properties of SnS, such as its high absorption coefficient, long carrier lifetime, and high quantum efficiency, make it a promising candidate for photocatalytic applications. Additionally, the abundance, low toxicity, and earth-abundant constituent elements of SnS make it a sustainable and environmentally friendly alternative to other photocatalytic materials. Further research is needed to optimize the photocatalytic performance of SnS and to develop efficient and stable SnS-based photocatalysts for practical applications (Nengzi *et al*. 2020; Hegde *et al*. 2021; Zhang *et al*. 2021; Alikarami *et al*. 2022; He *et al*. 2023; Katoch *et al*. 2023).

The process of doping photocatalysts involves adding impurities to improve their photocatalytic properties by altering their electronic structure and enhancing their ability to absorb light and generate charge carriers. Metals like silver, gold, and platinum and nonmetals like nitrogen and sulfur are common dopants used. Doping with strontium (Sr) has shown to significantly

enhance photocatalytic activity by improving visible light absorption and charge carrier separation, leading to applications in water splitting, pollutant degradation, and hydrogen production. Sr doping also improves stability and durability, making it a promising strategy for developing high-performance photocatalysts (Tran *et al*. 2020; Iqbal *et al*. 2021; Yarahmadi *et al*. 2021; Uma *et al*. 2022; Sharma *et al*. 2023).

In this work, we have successfully synthesized nanoflowers of SnS and Sr-doped SnS, which demonstrate excellent performance for the degradation of MNZ. The unique morphology of the nanoflowers provides a large surface area for the active sites to interact with the target pollutant, while the Sr doping enhances the catalytic activity and stability of the material. Our results suggest that the synthesized nanoflowers have great potential for the treatment of MNZ -contaminated wastewater, and may also inspire the development of new nanomaterials for environmental remediation.

2. EXPERIMENTAL

2.1. Catalyst preparation

In this study, a hydrothermal technique was employed to synthesize SnS and Sr-SnS NPs. Initially, SnS NPs were prepared by dissolving 2.25 g of $SnCl_2$ $2H_2O$ in 20 mL of distilled water (625 mM) and 4.5 g of $SC(NH_2)_2$ in 40 mL of distilled water (1.5M) separately. Each solution was stirred for 30 min. Next, the $SnCl_2$ $2H_2O$ solution was added to the SC $(NH_2)_2$ solutions, and the resulting mixture was stirred for a duration of 2 h, while introducing 20 mL of distilled water. The mixed solution is then transferred to a 100-mL Teflon-lined stainless steel autoclave and maintained at 180 °C for 12 h. The $Sn_{0.9}Sr_{0.1}S$ samples were synthesized using 62.5 mM of $SrCl_2$ $6H_2O$. After the reaction was completed, the autoclave was allowed to cool down to room temperature. To eliminate any remaining impurities, the resulting powder underwent multiple washes with ethanol and distilled water. Finally, the powder was air-dried for duration of 2 h at 50 °C.

2.2. Catalyst characterization

The X-ray diffraction (XRD) patterns and scanning electron microscope (SEM) micrographs of the samples prepared as mentioned above were recorded. The XRD patterns were recorded on a Siemens D-5000 diffractometer with Cu-Kα radiation ($\lambda =$ 1.5418 Å) and surface morphology was studied using SEM (Thermo Fisher Scientific). The UV–Vis absorption spectra were measured by UV–Vis spectrophotometer (Shimadzu UV-2401).

2.3. Photocatalytic removal studies

The photocatalytic process was conducted in batch mode at room temperature. MNZ solutions containing the desired concentrations (10, 20, and 30 mg/L) were prepared by dissolving the corresponding amount of MNZ in distilled water. The solution was transferred to a triple-walled Pyrex batch reactor and an appropriate amount of SnS and Sr-doped SnS (1 g/L) catalyst was determined to be the optimal dose, and was added. The pH of the solution was adjusted using NaOH or HCl. All mixtures were magnetically stirred. Each sample was kept in the dark for 30 min in order to reach adsorption-equilibrium, the reactor was then exposed to natural sunlight irradiation for 5 h. Sampling for analysis was affected by taking 3 mL aliquots from the reaction mixture at regular time intervals (30 min), subjected to vigorous centrifugation (6,000 rpm, 20 min) to remove the catalyst particles, and filtered through 0.45-mm millipore filters. Finally, the absorbance of the solution was measured at 320 nm. The percentage of degradation was estimated using the following equation:

$$\text{Degradation, } \% = \frac{C_0 - C_t}{C_0} \times 100 \tag{1}$$

where C_0 is the initial MNZ concentration and C_t is the MNZ concentration at certain reaction time t (min).

3. RESULTS AND DISCUSSION

3.1. Characterization of the catalyst

3.1.1. XRD analysis

The XRD patterns of SnS and Sr-doped SnS are depicted in Figure 1, with diffraction peaks located at 22.03°, 26.03°, 27.41°, 30.48°, 31.53°, 31.94°, 39.04°, 44.73°, 48.6°, 51.28°, 54.22°, and 64.20°. According to the JCPDS card (96-900-8786), these peaks have been identified as the orthorhombic structure's Bragg's planes (101), (201), (210), (011), (111), (400), (410), (411), (211), (151), (061), and (512), respectively (Baby *et al*. 2021; Dar *et al*. 2022). Furthermore, no additional

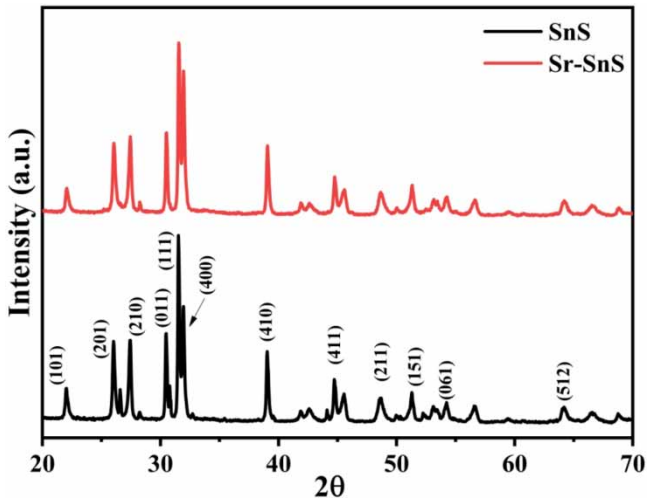

Figure 1 | XRD spectra of SnS and Sr-SnS nanoflowers.

strontium-related peaks showed up, proving that no new impurity phases have developed. An in-depth analysis of the XRD peaks (111) (400) (see supplementary material) of both SnS and Sr-SnS patterns showed a slight shift toward high diffraction angles (Figure 1), demonstrating the incorporation of Sr^{2+} in SnS substitutional sites. In addition, structural parameters such as average crystallite size, dislocation density, microstrain, and lattice parameters were calculated using the following equations, with the results shown in Table 1.

The mean crystallite size D of the synthesized nanoparticles was estimated from the full width half maximum FWHM (β) of all peaks, using the Debye–Scherer's formula (Salima *et al.* 2023):

$$D = \frac{0.9\,\lambda}{\beta \cos\theta} \tag{2}$$

where λ is the used wavelength ($\lambda = 1.5406$ Å) and θ is the Bragg's diffraction angle.

The crystallite mean size was estimated to 44 and 40 nm for both SnS and Sr-SnS, respectively. Moreover, the orthorhombic lattice parameters (a, b, and c) were determined using the following formula (Arefi-Rad & Kafashan 2020):

$$\frac{1}{d_{hkl}^2} = \frac{h^2}{a^2} + \frac{k^2}{b^2} + \frac{l^2}{c^2} \tag{3}$$

where 'd_{hkl}' represents the interplanar spacing, 'hkl' is the Miller indices. The planes (400), (011) and (101) were used for the calculation of lattice parameters a, b, and c, respectively. The dislocation density and microstrain were calculated using the following relations, respectively (Messai *et al.* 2023):

$$\delta = \frac{1}{D^2} \tag{4}$$

and

$$\varepsilon = \frac{\beta\,\cos\theta}{4} \tag{5}$$

Table 1 | Structural parameters of SnS and Sr-SnS nanoflowers

Samples	Diffraction angles	Crystallite size (nm)	Microstrain 10^{-3}	Dislocation density 10^{-3} (nm^{-2})	Lattice parameters (Å)		
					a	b	c
SnS	31.54	44	0.2151	0.5593	11.20	3.99	4.31
Sr-SnS	31.57	40	0.2309	0.6594	11.19	3.99	4.30

Table 1 shows that the diffraction peaks shift slightly toward the higher diffraction angles and the lattice parameters (a, c) are slightly decreased with increasing Sr^{2+} concentrations, despite the fact that the value of parameter b remains constant. These observations revealed that Sr^{2+} was successfully substituted into the SnS host. Additionally, we can see that Sr doping results in an increase in microstrain and dislocation density. These results being comparable with those observed on Sr-incorporated ZnS (Boulkroune *et al.* 2019).

3.1.2. Optical properties and band gap estimation

Figure 2 presents the optical properties of both undoped SnS and Sr-SnS NPs in the range of 200–700 nm. Upon Sr doping, a remarkable alteration in absorbance was evident, notably showcasing a shift toward higher longer wavelengths. This shift can be attributed to the incorporation of additional electrons during the Sr doping process, leading to a redistribution of energy levels within the crystal structure of the nanoparticles. The observed change in absorbance suggests a modification in the electronic band structure of the SnS nanoparticles due to Sr doping.

The doping also led to a change in the gap energy of SnS NPs. Gap energy is an essential characteristic that directly influences the electronic and optical properties of semiconductor materials. Commonly, the direct bandgap energy (E_g) is estimated via Tauc's relation $(F(R)hv)^2 = A\ (hv - E_g)$, which hv and A are incident photon energy and 'A' constant, respectively (Arefi-Rad & Kafashan 2020). The interception of the linear fit of $(F(R)\ hv)^2$ plot with hv axis shows the E_g (Salima *et al.* 2023).

Figure 3 displays the Tauc's plots for SnS and Sr-SnS NPs. The bandgap of SnS was measured to be 1.42 eV, whereas for Sr-SnS, it was found to be 1.48 eV. The same results have been documented (Hegde *et al.* 2020; Baby *et al.* 2021). The increase in the gap energy observed here can be attributed to the introduction of additional levels into the conduction band, effectively lowering the energy required to excite electrons in the material.

3.1.3. SEM analysis

The morphological analysis of SnS and Sr-doped SnS nanoparticles reveals intriguing and heterogeneous structures that hold significant potential for various surface applications, particularly in the realm of photocatalysis. In the case of pristine SnS nanoparticles, a rich diversity of morphologies is evident from the images, showcasing distinct nanoflower formation, along with nano-triangles and nano-plates that intricately assemble into flower-like structures. Similarly, the Sr-doped SnS nanoparticles exhibit striking resemblances in their morphologies, featuring nanoflower arrangements and nano-plates organized in captivating flower-like configurations (Figure 4) (Vaughn *et al.* 2012; Bai *et al.* 2021). These intricate morphologies play a pivotal role in dictating the nanoparticles' surface properties, making them highly promising candidates for photocatalytic applications. The heterogeneity of these morphologies not only enhances the surface area, but also influences the light absorption and charge separation capabilities, ultimately boosting the photocatalytic efficiency. The EDX profile (Figure 5) also proves the coexistence of Sn, S, and Sr elements.

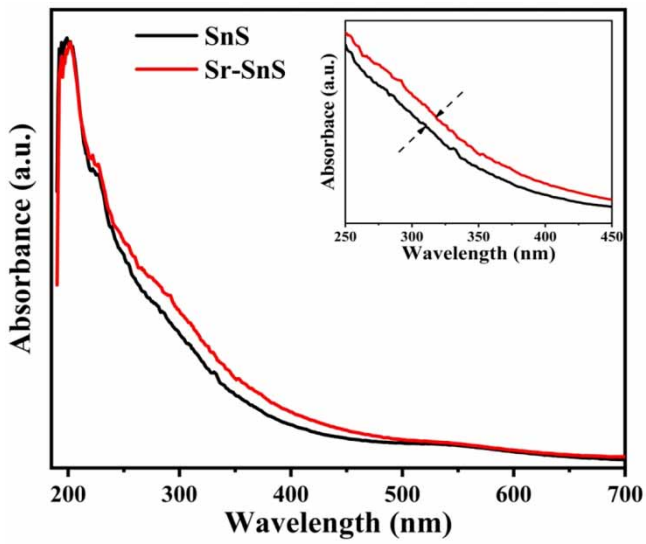

Figure 2 | UV–Visible spectra for SnS and doped Sr-SnS nanoflowers. The inset shows a shift toward longer wavelengths.

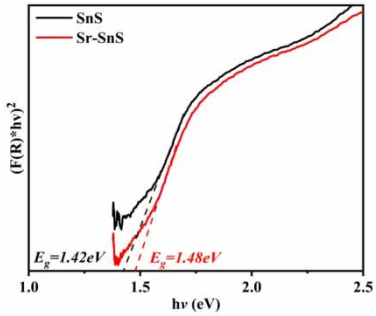

Figure 3 | Estimation of band gap for SnS and doped Sr-SnS nanoflowers using the Kubelka–Munk approach.

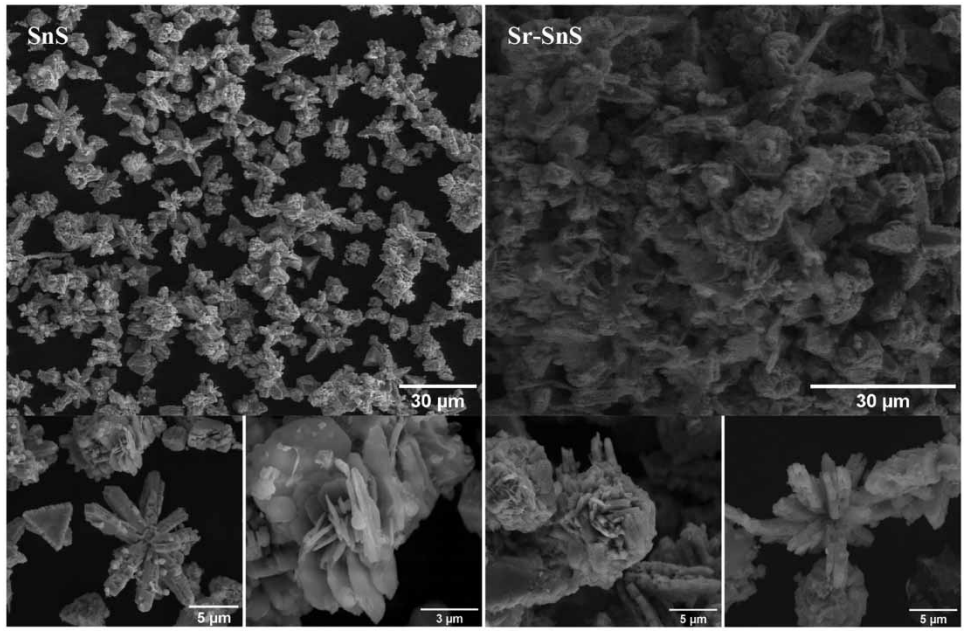

Figure 4 | SEM images for SnS and doped Sr-SnS nanoflowers.

3.2. Photodegradation of MNZ

3.2.1. Evaluation of the treatment strategy for MNZ degradation

In order to evaluate the effectiveness of photocatalysis, a series of preliminary tests were conducted. The objective was to study the degradation process of MNZ in polluted water using various experimental conditions. Three different approaches were considered, based on the use or absence of a catalyst (Sr-doped SnS) and a light source (sunlight). As a result, three distinct scenarios were analyzed: (1) without catalyst and without radiation, which corresponds to adsorption phenomena; (2) with catalyst and without radiation, which represents photolysis process, and (3) with catalyst and radiation, which corresponds to photocatalysis. Figure 6 illustrates the evolution of MNZ degradation under each of these three conditions.

The results of the experimental tests clearly indicate that photocatalysis has a substantial impact on the photodegradation of MNZ, while the effects of adsorption and photolysis are relatively insignificant. This finding is consistent with prior research in the field, which has already demonstrated the effectiveness of photocatalytic methods in removing pollutants from water. The use of a catalyst in combination with sunlight leads to a significant increase in the degradation rate of MNZ, highlighting the potential of photocatalysis as an efficient and sustainable method for water treatment. These results provide valuable insights into future research in the field of environmental engineering and water treatment (Chekir *et al.* 2017; Aoudjit *et al.* 2018; Bouarroudj *et al.* 2021).

Furthermore, after 300 min of exposure to sunlight in the presence of Sr-doped SnS catalyst nanoflowers, 91% of MNZ was degraded. In this experiment, we also studied the photocatalytic activity of pure SnS and Sr-doped SnS nanoparticles under

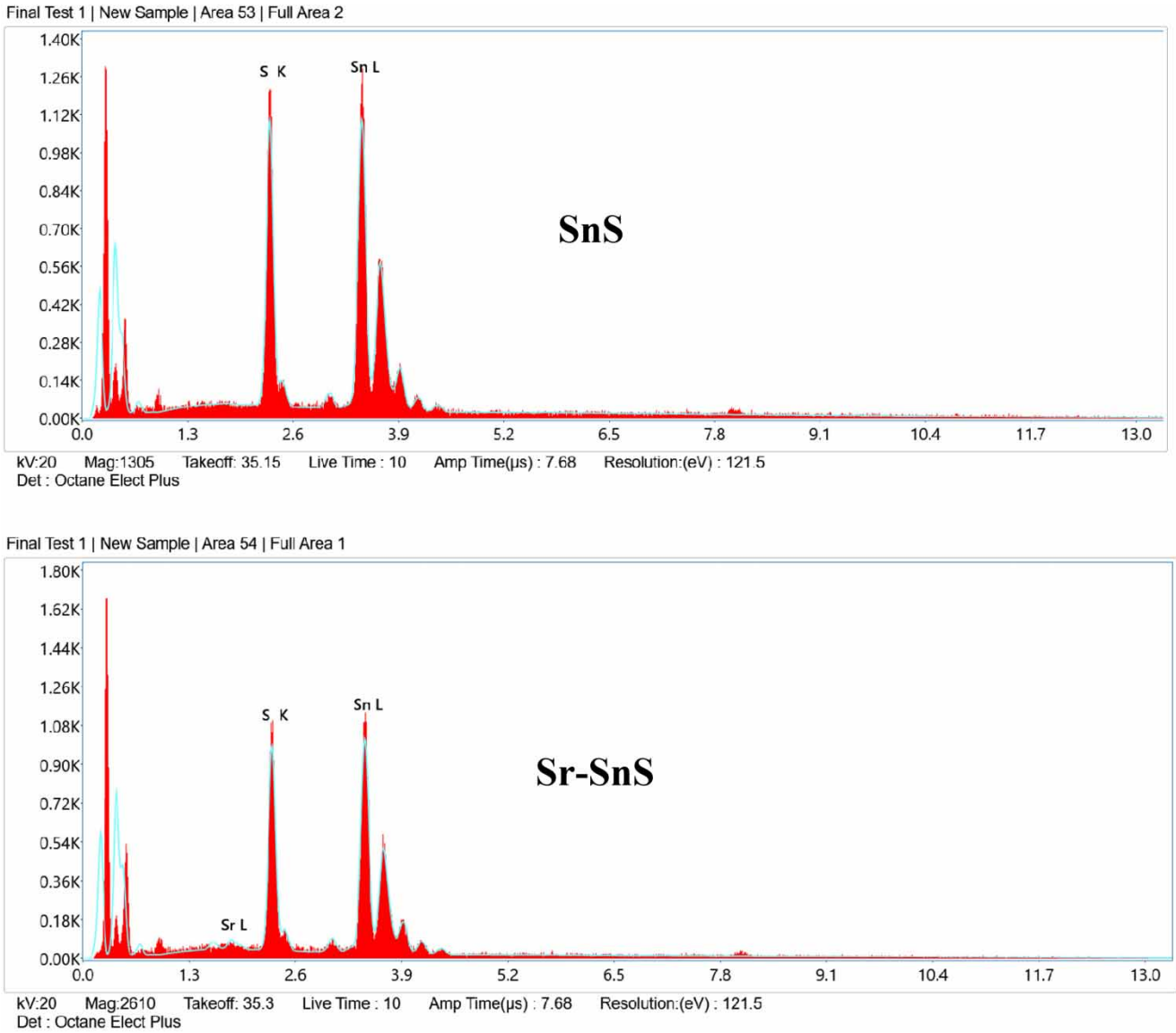

Figure 5 | EDS spectrum for SnS and doped Sr-SnS nanoflowers.

solar radiation. The results are presented in Figure 7. The study confirmed that Sr-doped SnS nanoparticles exhibit significantly higher photocatalytic activity than observed for pure SnS nanoparticles when exposed to sunlight. This remarkable improvement in photocatalytic activity is likely due to the decrease in the energy gap. UV–Vis analysis revealed this decrease, suggesting that the presence of Sr in the material's structure plays a key role in enhancing its ability to catalyze photochemical reactions. These results are promising and could have significant applications in the field of renewable energy production and environmental pollution remediation.

3.2.2. Radiation source

In a study on the photocatalytic degradation of MNZ using Sr-doped SnS photocatalyst; two different irradiation sources were employed. The first source was an artificial one, which emanated from a PHILPS PL-L 24 W/10/4P UV lamp with a maximum wavelength of 365 nm and an intensity of 18.6 W/m^2. The second source was solar UV radiation, which was measured using a Kipp & Zonzn CMP11 global UV radiometer with an intensity of 853 W/m^2. The results of the study, as shown in Figure 8, indicate that after 300 min of irradiation, the Sr-doped SnS Photocatalyst was able to degrade 91%

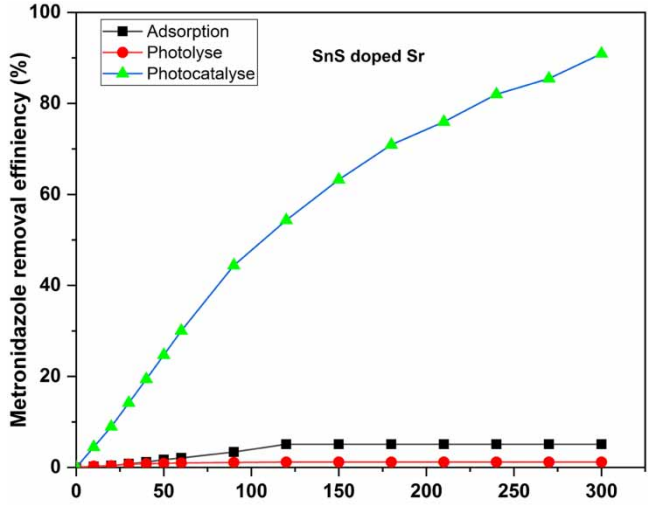

Figure 6 | Degradation of MNZ under different processes ($C_{MNZ} = 20$ mg/L, $C_{catalyst} = 1$ g/L and free pH = 6, 4).

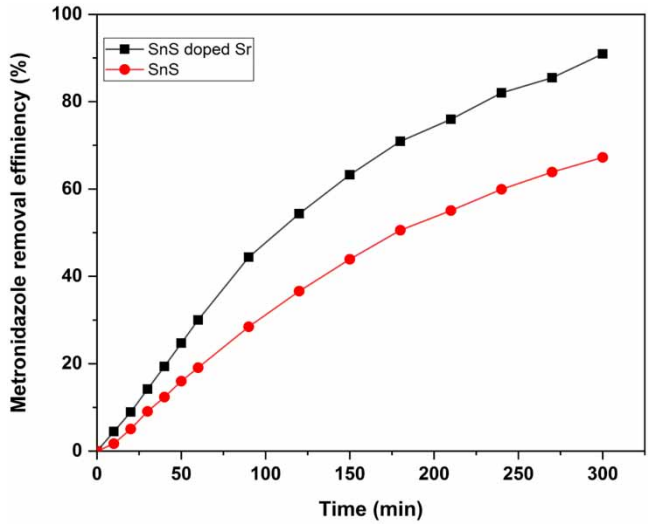

Figure 7 | Comparison of SnS and Sr-doped SnS photocatalytic activities under sunlight irradiation ($C_{MNZ} = 20$ mg/L, $C_{catalyst} = 1$ g/L and free pH).

of the MNZ under sunlight and 58% under UV lamp irradiation. The high level of MNZ degradation observed under natural sunlight using the Sr-doped SnS Photocatalyst suggests that it could be a promising material for the photocatalytic degradation of MNZ in wastewater treatment applications under natural sunlight.

The photocatalyst's ability to breakdown MNZ can be explained by its reaction with light. When the photocatalyst is exposed to light, electrons from the valence band move to the conduction band and holes are created in the valence band. This process generates photons that can reduce oxygen to create superoxide radicals ($O2^{-}$). In addition, the holes in the valence band can oxidize water molecules or (OH^{-}) ions to create hydroxyl radicals (OH•). These superoxide and hydroxyl radicals are involved in the breakdown of MNZ drugs. The photogenerated electrons that move to the conduction band are typically unstable and quickly return to the valence band, as has been demonstrated previously (Bouarroudj *et al*. 2021, 2023).

3.2.3. Effect of pH

The pH of the solution is a crucial factor that affects the rate of degradation of organic compounds in the photocatalytic process, and it is also an important operational parameter in wastewater treatments (Wu *et al*. 2001; Saien & Soleymani 2007). Figure 9 illustrates the impact of pH on the photocatalytic degradation of MNZ. The results show that the degradation efficiency of MNZ

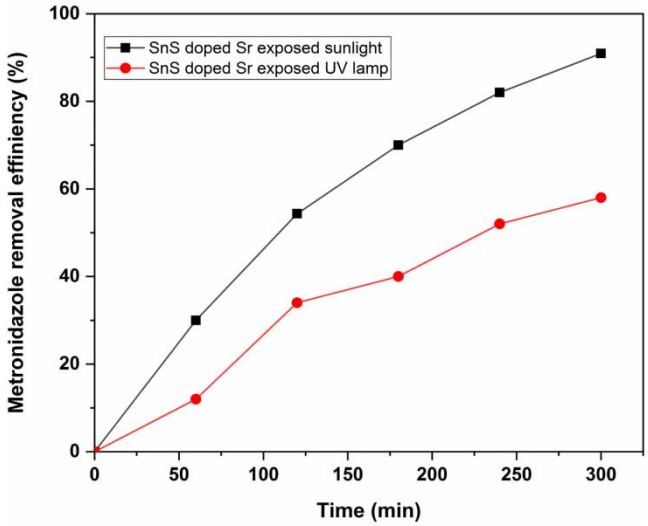

Figure 8 | Comparison of degradation of MNZ exposed to different sources of light ($C_{MNZ} = 20$ mg/L, $C_{catalyst} = 1$ g/L and free pH = 6, 4).

remains relatively stable at pH values between 3 and 6.4. However, the degradation efficiency at a pH value of 10 is significantly lower than those observed at the appropriate pH values. This is likely due to the fact that at high pH values, the MNZ molecules dissociate into their respective ions, which can decrease the interaction between the photocatalyst and the MNZ molecules, thus reducing the degradation efficiency. Therefore, optimizing the pH of the solution is critical to achieving optimal photocatalytic degradation efficiency of MNZ in wastewater treatments. The photocatalytic degradation of MNZ is generally higher at an acidic pH than at a basic pH due to the limited solubility of MNZ in water at high pH. At a basic pH, MNZ can dissociate into ions that are less likely to interact with the photocatalyst. On the other hand, at an acidic pH, MNZ remains primarily in its molecular form, which increases its reactivity with the photocatalyst. Additionally, the production of hydroxyl radicals (OH•) is higher at an acidic pH due to the increased concentration of protons (H+) in the solution, which promotes the photocatalytic degradation of MNZ (Farzadkia *et al*. 2015; Ayanda *et al*. 2023).

3.2.4. Effect of concentration

The study of the influence of the initial concentration of pollutants on the efficiency of photocatalysis is crucial in determining the optimal conditions for the degradation of pollutants. In this experiment, we investigated the effect of varying the initial

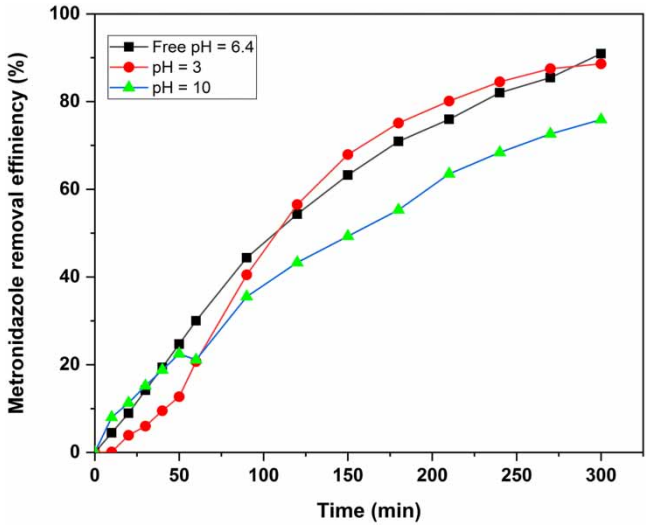

Figure 9 | Sunlight photodegradation of MNZ at different pH values ($C_{MNZ} = 20$ mg/L and $C_{catalyst} = 1$ g/L).

concentration of MNZ on the degradation rate of the pollutant using photocatalysis. The experiment was carried out at a free pH of 6.4 and a dose of 1 g of Sr-doped SnS photocatalyst. We monitored the degradation rate of MNZ over a period of 300 min for initial concentrations ranging from 20 to 40 mg/L. The results were plotted on a curve shown in Figure 10, which clearly shows the degradation rate of MNZ decreasing as the initial concentration of the pollutant increases. The findings of the study demonstrate that the degradation of MNZ is significantly affected by the initial concentration of the substrate. The results reveal that the degradation rate of the pollutant is higher when the initial concentration is lower. Specifically, when the initial concentration is at 20 mg/L, the degradation rate is remarkably high and yields about 91% after 300 min of solar irradiation. However, when the initial concentration is increased to 30 and 40 mg/L, the degradation rate decreases from 82 to 76%, respectively. These results suggest that the efficiency of degradation decreases as the pollutant concentrations increase. These findings are consistent with those reported in previous studies, which reinforce the notion that the initial concentration of the pollutant plays a crucial role in the effectiveness of the degradation process (Aoudjit *et al*. 2021, 2020, 2022; Ghribi *et al*. 2020). One possible explanation for this phenomenon is that increasing the initial concentration of the pollutant can lead to saturation of the active sites on the photocatalyst, which limits the photocatalyst's ability to degrade the pollutant. In other words, when the initial concentration of the pollutant is too high, there is increased competition for the active sites on the photocatalyst surface, which reduces the efficiency of the photocatalytic degradation. Furthermore, at high pollutant concentrations, there may be formation of intermediate products that can inhibit the photocatalytic degradation reaction. These intermediate products can adsorb onto the photocatalyst surface and block the active sites, thereby reducing the degradation efficiency. Moreover, the inner filtration effect occurs when the concentration of MNZ increases in a photocatalytic system, leading to a higher likelihood of UV light being absorbed by the MNZ molecules before reaching the photocatalyst surface. This results in a reduction in the number of photons that can reach the photocatalyst, potentially decreasing the efficiency of the photocatalytic process (Chatzitakis *et al*. 2008; Palominos *et al*. 2009; Wang *et al*. 2010; Prados-Joya *et al*. 2011; Farzadkia *et al*. 2015).

3.2.5. Effect of catalyst dose

In order to determine the ideal amount of catalyst for achieving maximum photocatalytic degradation, a range of catalyst amounts were tested, varying from 0.1 to 1 g/L. The concentration of MNZ used in the experiment was held constant at 20 mg/L. The results of this investigation are displayed in Figure 11.

The experimental results clearly demonstrate a positive correlation between the quantity of catalyst used and the rate of degradation of MNZ. The rate of degradation increased in proportion to the quantity of the catalyst used, with a yield of 91% after 300 min when a 1 g/L catalyst dose was utilized. This suggests that the yield of the photodegradation process is directly proportional to the amount of catalyst used. One possible explanation for this phenomenon is that the increase in

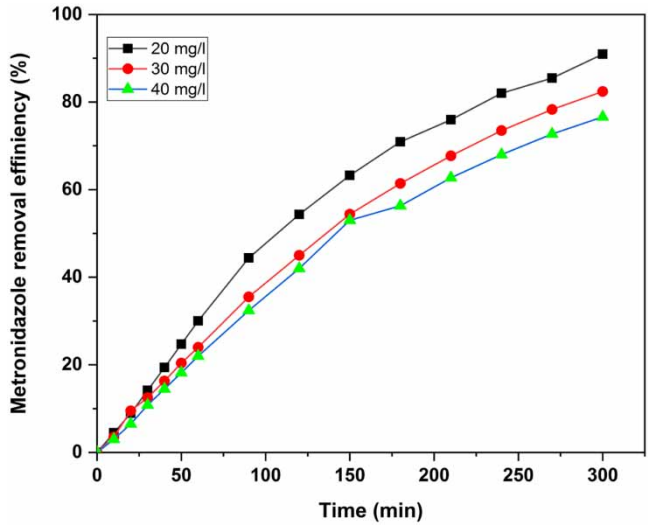

Figure 10 | Photodegradation of MNZ with time at, different concentrations of MNZ, under sunlight irradiation ($C_{catalyst} = 1$ g/L and free pH = 6, 4).

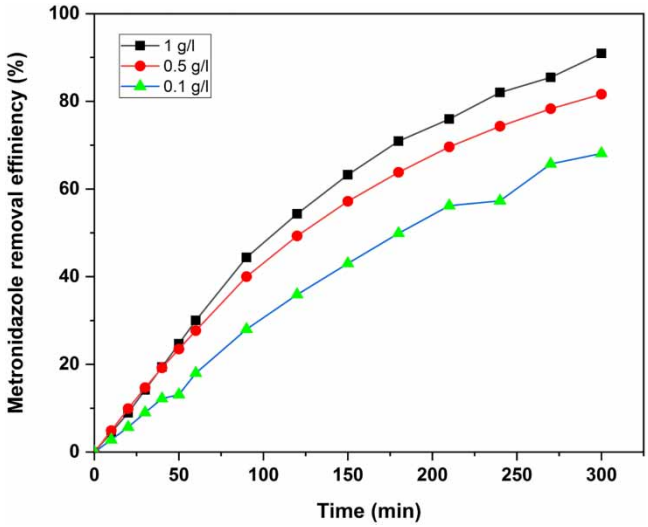

Figure 11 | Photodegradation of MNZ at different doses of Sr-doped SnS catalyst, under sunlight irradiation ($C_{MNZ} = 20$ mg/L and free pH = 6.4).

active sites available for the production of OH^- free radicals is responsible for the degradation of MNZ. Thus, using higher quantities of catalyst could result in more efficient and effective degradation of MNZ in wastewater treatment. However, excessive formation of free radicals can occur if the dose of photocatalyst is too high. This excessive formation of free radicals can combine and react with other species present in the solution, thereby reducing their effectiveness in degrading MNZ (Kaur & Singhal 2014; Farzadkia *et al*. 2015; Kumar & Kumar 2019; Bouarroudj *et al*. 2023).

3.2.6. Reuse of photocatalyst

In order to ensure that a photocatalyst is economically feasible, it is important that it is stable and can be reused for multiple cycles. To test this, several experiments were conducted using the Sr-doped SnS catalyst for the degradation of MNZ. The recovered catalyst was used for four cycles, with an adsorption time of 300 min followed by photocatalysis at optimum conditions. The results, as shown in Figure 12, indicate that even after repeated cycles, the catalyst remained active with only a slight decrease in MNZ degradation, from 91 to 83% after a repeated cycle. This demonstrates the potential for the synthesized photocatalyst to be both effective and economically viable for use in environmental remediation processes.

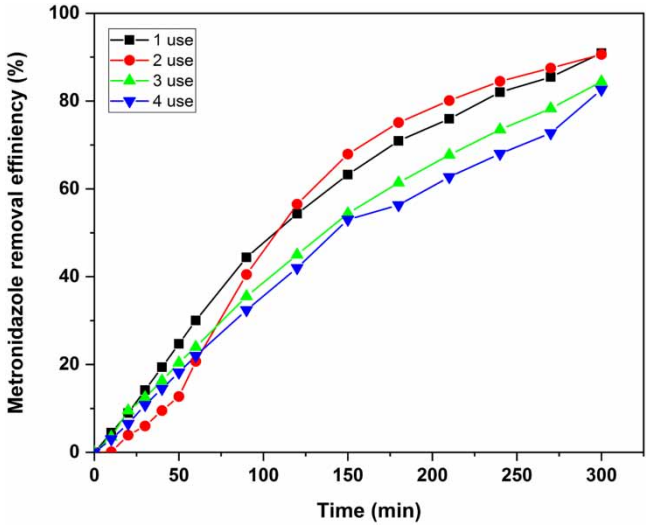

Figure 12 | Photodegradation of MNZ over four catalytic cycles in sunlight, (20 mg/L, free pH = 6.4, and $C_{catalyst} = 1$ g/L).

It is possible that the efficiency of photocatalytic degradation decreases at 82% after several cycles of use, particularly after the fourth cycle of reuse. This decrease can be caused by several factors, such as the accumulation of contaminants on the surface of the catalyst, the physical or chemical deterioration of the catalyst, and the loss of active surface area of the catalyst. Organic contaminants can accumulate on the surface of the catalyst, reducing its efficiency, despite cleaning between use cycles. Additionally, the catalyst can undergo physical or chemical degradation over time, which can also reduce its efficiency. Finally, the active surface area of the catalyst can decrease due to the formation of passive layers or a decrease in specific surface area, which can also reduce the efficiency of degradation (Chakrabarti & Dutta 2004; Yu *et al*. 2016; Anjum *et al*. 2017; Zhao *et al*. 2018).

4. CONCLUSION

In conclusion, the synthesis of strontium-doped SnS nanoflowers using the solvothermal method has been successfully achieved. The structural analysis confirmed the successful substitution of Sr^{2+} ions into the SnS host lattice, resulting in a decrease in lattice parameter and a slight shift in diffraction peaks. Furthermore, the UV–Vis investigations revealed an increased band gap of Sr-doped SnS, with an estimated value of 1.48 eV, indicating improved photocatalytic properties.

The photocatalytic abilities of Sr-doped SnS were assessed through the degradation of MNZ under natural sunlight. The results demonstrated that the optimal conditions for MNZ degradation were a free pH of 6.4, a dye concentration of 20 mg/L, and a catalyst dose of 1 g/L. Remarkably, the Sr-doped SnS catalyst exhibited an impressive degradation efficiency, with 91% degradation of MNZ achieved under natural sunlight irradiation. Importantly, the catalyst maintained its photodegradation capacity even after multiple treatment cycles, highlighting its stability and reusability.

These findings contribute to the growing body of knowledge on the synthesis and characterization of doped semiconductor nanomaterials for environmental applications. The successful synthesis of strontium-doped SnS nanoflowers with enhanced photocatalytic properties opens up possibilities for their use in various fields, including wastewater treatment and environmental remediation. Further research and optimization of the synthesis process can lead to the development of even more efficient and sustainable photocatalytic materials for addressing environmental challenges.

ACKNOWLEDGEMENTS

The authors of this manuscript would like to thank the General Directorate for Scientific Research and Technological Development (DGRSDT) and the Ministry of Higher Education and Scientific Research (MESRS), Algeria, for funding this project.

DATA AVAILABILITY STATEMENT

All relevant data are included in the paper or its Supplementary Information.

CONFLICT OF INTEREST

The authors declare there is no conflict.

REFERENCES

Akhtar, N., Syakir Ishak, M. I., Bhawani, S. A. & Umar, K. 2021 Various natural and anthropogenic factors responsible for water quality degradation: A review. *Water* **13** (19), 2660. https://doi.org/10.3390/w13192660.

Alikarami, S., Soltanizade, A. & Rashchi, F. 2022 Synthesis of CdS–SnS photocatalyst by chemical co-precipitation for photocatalytic degradation of methylene blue and rhodamine B under irradiation by visible light. *Journal of Physics and Chemistry of Solids* **171**, 110993. https://doi.org/10.1016/j.jpcs.2022.110993.

Anjum, M., Kumar, R. & Barakat, M. A. 2017 Visible light driven photocatalytic degradation of organic pollutants in wastewater and real sludge using ZnO–ZnS/Ag_2O–Ag_2S nanocomposite. *Journal of the Taiwan Institute of Chemical Engineers* **77**, 227–235. https://doi.org/10.1016/j.jtice.2017.05.007.

Aoudjit, L., Martins, P. M., Madjene, F., Petrovykh, D. Y. & Lanceros-Mendez, S. 2018 Photocatalytic reusable membranes for the effective degradation of tartrazine with a solar photoreactor. *Journal of Hazardous Materials* **344**, 408–416. https://doi.org/10.1016/j.jhazmat.2017.10.053.

Aoudjit, L., Salazar, H., Zioui, D., Sebti, A., Martins, P. M. & Lanceros-Méndez, S. 2021 Reusable Ag@TiO2-Based photocatalytic nanocomposite membranes for solar degradation of contaminants of emerging concern. *Polymers* **13**, 3718. https://doi.org/10.3390/polym13213718.

Aoudjit, F., Touahra, F., Aoudjit, L., Cherifi, O. & Halliche, D. 2020 Efficient solar heterogeneous photocatalytic degradation of metronidazole using heterojunction semiconductors hybrid nanocomposite, layered double hydroxides. *Water Science and Technology* **82** (12), 2837–2846. https://doi.org/10.2166/wst.2020.519.

Aoudjit, L., Salazar, H., Zioui, D., Sebti, A., Martins, P. M. & Lanceros-Méndez, S. 2022 Solar photocatalytic membranes: an experimental and artificial neural network modeling approach for niflumic acid degradation. *Membranes* **12** (9), 849. https://doi.org/10.3390/membranes12090849.

Aoudjit, L., Nabbat, E. A. & Zioui, D. 2023 Chitosan/ZnO nanocomposite membranes for removal of paracetamol from water. *Cellulose Chem. Technol.* **57**, 437. https://doi.org/10.35812/CelluloseChemTechnol.2023.57.39.

Arefi-Rad, M. R. & Kafashan, H. 2020 Pb-doped SnS nano-powders: Comprehensive physical characterizations. *Optical Materials* **105**, 109887. https://doi.org/10.1016/j.optmat.2020.109887.

Ayanda, O. S., Adeleye, B. O., Aremu, O. H., Ojobola, F. B., Lawal, O. S., Amodu, O. S., Oketayo, O. O., Klink, M. J. & Nelana, S. M. 2023 Photocatalytic degradation of metronidazole using zinc oxide nanoparticles supported on acha waste. *Indonesian Journal of Chemistry* **23** (1), 158. https://doi.org/10.22146/ijc.75585.

Baaloudj, O., Assadi, I., Nasrallah, N., El Jery, A., Khezami, L. & Assadi, A. A. 2021 Simultaneous removal of antibiotics and inactivation of antibiotic-resistant bacteria by photocatalysis: A review. *Journal of Water Process Engineering* **42**, 102089. https://doi.org/10.1016/j.jwpe.2021.102089.

Baby, B. H., Philipson, A. & D., B. M. 2021 Temperature-assisted mechanochemically synthesized Cu and In doped SnS nanoparticles for thin film photovoltaics: Structure, phase stability and optoelectronic properties. *Optik* **240**, 166848. https://doi.org/10.1016/j.ijleo.2021.166848.

Bai, Y., Qin, Y. & Qiu, P. 2021 Boosting the acetone sensing of SnS nanoflakes by spin Mn substitution: A novel adsorption–desorption perspective. *Environmental Science: Nano* **8** (4), 1096–1108. https://doi.org/10.1039/D0EN01251C.

Bashir, I., Lone, F. A., Bhat, R. A., Mir, S. A., Dar, Z. A., Dar, S. A., 2020 Concerns and Threats of Contamination on Aquatic Ecosystems. In: *Bioremediation and Biotechnology* (Hakeem, K. R., Bhat, R. A. & Qadri, H. eds.). Springer International Publishing, Cham, Switzerland, pp. 1–26.

Bashiri, F., Khezri, S. M., Kalantary, R. R. & Kakavandi, B. 2020 Enhanced photocatalytic degradation of metronidazole by TiO2 decorated on magnetic reduced graphene oxide: characterization, optimization and reaction mechanism studies. *Journal of Molecular Liquids* **314**, 113608. https://doi.org/10.1016/j.molliq.2020.113608.

Bouarroudj, T., Aoudjit, L., Djahida, L., Zaidi, B., Ouraghi, M., Zioui, D., Mahidine, S., Shekhar, C. & Bachari, K. 2021 Photodegradation of tartrazine dye favored by natural sunlight on pure and (Ce, Ag) co-doped ZnO catalysts. *Water Science and Technology* **83** (9), 2118–2134. https://doi.org/10.2166/wst.2021.106.

Bouarroudj, T., Aoudjit, L., Nessaibia, I., Zioui, D., Messai, Y., Bendjama, A., Mezrag, S., Chabbi, M. & Bachari, K. 2023 Enhanced photocatalytic activity of Ce and Ag Co-doped ZnO nanorods of paracetamol and metronidazole antibiotics Co-Degradation in wastewater promoted by solar light. *Russian Journal of Physical Chemistry A* **97** (5), 1074–1087. https://doi.org/10.1134/S0036024423050278.

Boulkroune, R., Sebais, M., Messai, Y., Bourzami, R., Schmutz, M., Blanck, C., Halimi, O. & Boudine, B. 2019 Hydrothermal synthesis of strontium-doped ZnS nanoparticles: Structural, electronic and photocatalytic investigations. *Bulletin of Materials Science* **42** (5), 223. https://doi.org/10.1007/s12034-019-1905-2.

Castiglioni, M., Rivoira, L., Ingrando, I., Meucci, L., Binetti, R., Fungi, M., El-Ghadraoui, A., Bakari, Z., Del Bubba, M. & Bruzzoniti, M. C. 2022 Biochars intended for water filtration: A comparative study with activated carbons of their physicochemical properties and removal efficiency towards neutral and anionic organic pollutants. *Chemosphere* **288**, 132538. https://doi.org/10.1016/j.chemosphere.2021.132538.

Chakrabarti, S. & Dutta, B. 2004 Photocatalytic degradation of model textile dyes in wastewater using ZnO as semiconductor catalyst. *Journal of Hazardous Materials* **112** (3), 269–278. https://doi.org/10.1016/j.jhazmat.2004.05.013.

Chatzitakis, A., Berberidou, C., Paspaltsis, I., Kyriakou, G., Sklaviadis, T. & Poulios, I. 2008 Photocatalytic degradation and drug activity reduction of Chloramphenicol. *Water Research* **42** (1–2), 386–394. https://doi.org/10.1016/j.watres.2007.07.030.

Chekir, N., Tassalit, D., Benhabiles, O., Kasbadji Merzouk, N., Ghenna, M., Abdessemed, A. & Issaadi, R. 2017 A comparative study of tartrazine degradation using UV and solar fixed bed reactors. *International Journal of Hydrogen Energy* **42** (13), 8948–8954. https://doi.org/10.1016/j.ijhydene.2016.11.057.

Chowdhary, P., Bharagava, R. N., Mishra, S., Khan, N., 2020 Role of Industries in Water Scarcity and Its Adverse Effects on Environment and Human Health. In: *Environmental Concerns and Sustainable Development* (Shukla, V. & Kumar, N. eds.). Springer Singapore, Singapore, pp. 235–256.

Dar, M. A., Govindarajan, D., Batoo, K. M. & Siva, C. 2022 Supercapacitor and magnetic properties of Fe doped SnS nanoparticles synthesized through solvothermal method. *Journal of Energy Storage* **52**, 105034. https://doi.org/10.1016/j.est.2022.105034.

Farzadkia, M., Bazrafshan, E., Esrafili, A., Yang, J.-K. & Shirzad-Siboni, M. 2015 Photocatalytic degradation of Metronidazole with illuminated TiO_2 nanoparticles. *Journal of Environmental Health Science and Engineering* **13** (1), 35. https://doi.org/10.1186/s40201-015-0194-y.

Ghribi, F., Sehailia, M., Aoudjit, L., Touahra, F., Zioui, D., Boumechhour, A., Halliche, D., Bachari, K. & Benmaamar, Z. 2020 Solar-light promoted photodegradation of metronidazole over ZnO-$ZnAl_2O_4$ heterojunction derived from 2D-layered double hydroxide structure. *Journal of Photochemistry and Photobiology A: Chemistry* **397**, 112510. https://doi.org/10.1016/j.jphotochem.2020.112510.

He, X., He, T., Xia, R., Qi, Y., Zhou, Y., Song, B., Liao, F., Kang, Z. & Jiang, L. 2023 SnS2/SnS heterojunction: An all-weather-active photocatalyst for Cr(VI) removal. *Separation and Purification Technology* **324**, 124515. https://doi.org/10.1016/j.seppur.2023.124515.

Hegde, S. S., Murahari, P., Fernandes, B. J., Venkatesh, R. & Ramesh, K. 2020 Synthesis, thermal stability and structural transition of cubic SnS nanoparticles. *Journal of Alloys and Compounds* **820**, 153116. https://doi.org/10.1016/j.jallcom.2019.153116.

Hegde, S. S., Surendra, B. S., Priyanka, V. P., Murahari, P. & Ramesh, K. 2021 Sns/LDPE Composite: A reusable floating photocatalyst for solar degradation of organic dyes. *Materials Today: Proceedings* **47**, 4255–4261. https://doi.org/10.1016/j.matpr.2021.04.567.

Hu, Z., Guan, D., Sun, Z., Zhang, Z., Shan, Y., Wu, Y., Gong, C. & Ren, X. 2023 Osmotic cleaning of typical inorganic and organic foulants on reverse osmosis membrane for textile printing and dyeing wastewater treatment. *Chemosphere* **336**, 139162. https://doi.org/10.1016/j.chemosphere.2023.139162.

Huang, Y., Li, Q., Guan, Z., Xia, D. & Wu, Z. 2023 Copper ferrite modified catalytic ceramic membrane for effective pollutant degradation and membrane fouling alleviation: The coupling of peroxymonosulfate activation and membrane filtration. *Journal of Water Process Engineering* **52**, 103564. https://doi.org/10.1016/j.jwpe.2023.103564.

Ighalo, J. O., Igwegbe, C. A., Adeniyi, A. G., Adeyanju, C. A. & Ogunniyi, S. 2020 Mitigation of Metronidazole (Flagyl) pollution in aqueous media by adsorption: A review. *Environmental Technology Reviews* **9** (1), 137–148. https://doi.org/10.1080/21622515.2020.1849409.

Igoud, S., Boutra, B., Aoudjit, L., Sebti, A., Khene, F., Bedrici, F. & Guernanou, R. 2019 Solar Wastewater Treatment: Advantages and Efficiency for Reuse in Agriculture and Industry. In *2019 7th International Renewable and Sustainable Energy Conference (IRSEC)*. IEEE, Agadir, Morocco.

Igoud, S., Zeriri, D., Aoudjit, L., Boutra, B., Sebti, A., Khene, F. & Mameche, A. 2021 Climate change adaptation by solar wastewater treatment (SOWAT) for reuse in agriculture and industry. *Irrigation and Drainage* **70** (2), 243–253. https://doi.org/10.1002/ird.2540.

Iqbal, S., Bahadur, A., Javed, M., Hakami, O., Irfan, R. M., Ahmad, Z., AlObaid, A., Al-Anazy, M. M., Baghdadi, H. B., Abd-Rabboh, H. S. M., Al-Muhimeed, T. I., Liu, G. & Nawaz, M. 2021 Design Ag-doped ZnO heterostructure photocatalyst with sulfurized graphitic c3n4 showing enhanced photocatalytic activity. *Materials Science and Engineering: B* **272**, 115320. https://doi.org/10.1016/j.mseb.2021.115320.

Igoud, S., Zeriri, D., Boutra, B., Mameche, A., Benzegane, Y., Belloula, M., Benkara, L., Aoudjit, L. & Sebti, A. 2022 Compared efficiency of sustainable and conventional treatments of saline oily wastewater rejected by petroleum industry in Algerian Sahara. *Petroleum Science and Technology* **40** (1), 92–106. https://doi.org/10.1080/10916466.2021.2002358.

Jovanovic, O., Amábile-Cuevas, C. F., Shang, C., Wang, C. & Ngai, K. W. 2021 What water professionals should know about antibiotics and antibiotic resistance: An overview. *ACS ES&T Water* **1** (6), 1334–1351. https://doi.org/10.1021/acsestwater.0c00308.

Karri, R. R., Ravindran, G. & Dehghani, M. H. 2021 Wastewater – Sources, Toxicity, and Their Consequences to Human Health. In: Karri, R. R., Ravindran, G. & Dehghani, M. H. (eds) *Soft Computing Techniques in Solid Waste and Wastewater Management*. Elsevier, London, UK, pp. 3–33. http://dx.doi.org/10.1016/B978-0-12-824463-0.00001-X.

Katoch, V., Singh, M., Katoch, A. & Prakash, B. 2023 Cost-effective microreactors for the synthesis of SnS nanoparticles and inline photocatalytic degradation of azo dyes. *Materials Letters* **333**, 133677. https://doi.org/10.1016/j.matlet.2022.133677.

Kaur, J. & Singhal, S. 2014 Facile synthesis of ZnO and transition metal doped ZnO nanoparticles for the photocatalytic degradation of Methyl Orange. *Ceramics International* **40** (5), 7417–7424. https://doi.org/10.1016/j.ceramint.2013.12.088.

Kiliç, Z. 2021 *Su Kirliliği Nedenleri, Olumsuz Etkileri ve Önleme Yöntemleri*. https://doi.org/10.47769/izufbed.862679. İstanbul Sabahattin Zaim Üniversitesi Fen Bilimleri Enstitüsü Dergisi.

Kumar, T. K. M. P. & Kumar, S. K. A. 2019 Visible-light-induced degradation of rhodamine B by nanosized ag2s-ZnS loaded on cellulose. *Photochemical & Photobiological Sciences* **18** (1), 148–154. https://doi.org/10.1039/c8pp00330k.

Li, J., Li, Y., Zhu, M., Mei, Q., Tang, X., Wu, Y., Yue, S., Tang, Y. & Wang, Q. 2023 Constructing aloe-emodin/FeOOH organic-inorganic heterojunction for synergetic photocatalysis-Fenton eliminating antibiotic pollutants. *Journal of Environmental Chemical Engineering* **11** (3), 109775. https://doi.org/10.1016/j.jece.2023.109775.

Liao, D., Chen, Y., Yin, F., Lv, B., Wu, F., Xie, J. & Feng, D. 2023 Performance of electrochemical treatment of refractory organic matter in printing and dyeing reverse osmosis concentrate. *Journal of Environmental Chemical Engineering* **11** (1), 109173. https://doi.org/10.1016/j.jece.2022.109173.

Lincho, J., Domingues, E., Mazierski, P., Miodyńska, M., Klimczuk, T., Zaleska-Medynska, A., Martins, R. C. & Gomes, J. 2023 The role of noble metals in TiO2 Nanotubes for the abatement of parabens by photocatalysis, catalytic and photocatalytic ozonation. *Separation and Purification Technology* 124747. https://doi.org/10.1016/j.seppur.2023.124747

Liu, C., Zhu, C., Wang, H., Xie, S., Zhou, J. & Fang, H. 2022 Synergistic removal of organic pollutants by Co-doped MIL-53(Al) composite through the integrated adsorption/photocatalysis. *Journal of Solid State Chemistry* **316**, 123582. https://doi.org/10.1016/j.jssc.2022.123582.

Liu, J., Zhang, S., Wang, W. & Zhang, H. 2023 Photoelectrocatalytic principles for meaningfully studying photocatalyst properties and photocatalysis processes: From fundamental theory to environmental applications. *Journal of Energy Chemistry* S2095495623003947. https://doi.org/10.1016/j.jechem.2023.06.038.

Martins, P. M., Salazar, H., Aoudjit, L., Gonçalves, R., Zioui, D., Fidalgo-Marijuan, A., Costa, C. M., Ferdov, S. & Lanceros-Mendez, S. 2021 Crystal morphology control of synthetic giniite for enhanced photo-Fenton activity against the emerging pollutant metronidazole. *Chemosphere* **262**, 128300. https://doi.org/10.1016/j.chemosphere.2020.128300.

Messai, Y., Bezzi, H., Bourzami, R., Chetoui, A., Bouarroudj, T., Tlili, S., Tairi, L., Belghidoum, A. & Ouksel, L. 2023 Investigation of structural, morphological, and photoluminescence properties of $Zn_{1-x}MG_xS$ nanoparticles prepared by solvothermal method: Insight from experimental and DFT study. *Russian Journal of Physical Chemistry A* **97** (8), 1769–1778. https://doi.org/10.1134/S0036024423080320.

Morin-Crini, N., Lichtfouse, E., Liu, G., Balaram, V., Ribeiro, A. R. L., Lu, Z., Stock, F., Carmona, E., Teixeira, M. R., Picos-Corrales, L. A., Moreno-Piraján, J. C., Giraldo, L., Li, C., Pandey, A., Hocquet, D., Torri, G. & Crini, G. 2022 Worldwide cases of water pollution by emerging contaminants: A review. *Environmental Chemistry Letters* **20** (4), 2311–2338. https://doi.org/10.1007/s10311-022-01447-4.

Nengzi, L., Yang, H., Hu, J., Zhang, W. & Jiang, D. 2020 Fabrication of SnS/TiO2 NRs/NSs photoelectrode as photoactivator of peroxymonosulfate for organic pollutants elimination. *Separation and Purification Technology* **249**, 117172. https://doi.org/10.1016/j.seppur.2020.117172.

Palominos, R. A., Mondaca, M. A., Giraldo, A., Peñuela, G., Pérez-Moya, M. & Mansilla, H. D. 2009 Photocatalytic oxidation of the antibiotic tetracycline on TiO_2 and ZnO suspensions. *Catalysis Today* **144** (1–2), 100–105. https://doi.org/10.1016/j.cattod.2008.12.031.

Pezeshki, H., Hashemi, M. & Rajabi, S. 2023 Removal of arsenic as a potentially toxic element from drinking water by filtration: A mini review of nanofiltration and reverse osmosis techniques. *Heliyon* **9** (3), e14246. https://doi.org/10.1016/j.heliyon.2023.e14246.

Polianciuc, S. I., Gurzău, A. E., Kiss, B., Ștefan, M. G. & Loghin, F. 2020 *Antibiotics in the Environment: Causes and Consequences*. Medicine and Pharmacy Reports **93** (3), 231–240.

Prados-Joya, G., Sánchez-Polo, M., Rivera-Utrilla, J. & Ferro-garcía, M. 2011 Photodegradation of the antibiotics nitroimidazoles in aqueous solution by ultraviolet radiation. *Water Research* **45** (1), 393–403. https://doi.org/10.1016/j.watres.2010.08.015.

Qadri, H., Bhat, R. A., Mehmood, M. A. & Dar, G. H. 2020 *Fresh Water Pollution Dynamics and Remediation*. Springer Singapore, Singapore.

Rokkarukala, S., Cherian, T., Ragavendran, C., Mohanraju, R., Kamaraj, C., Almoshari, Y., Albariqi, A., Sultan, M. H., Alsalhi, A. & Mohan, S. 2023 One-pot green synthesis of gold nanoparticles using Sarcophyton crassocaule, a marine soft coral: Assessing biological potentialities of antibacterial, antioxidant, anti-diabetic and catalytic degradation of toxic organic pollutants. *Heliyon* **9** (3), e14668. https://doi.org/10.1016/j.heliyon.2023.e14668.

Saien, J. & Soleymani, A. R. 2007 Degradation and mineralization of Direct Blue 71 in a circulating upflow reactor by UV/TiO2 process and employing a new method in kinetic study. *Journal of Hazardous Materials* **144** (1–2), 506–512. https://doi.org/10.1016/j.jhazmat.2006.10.065.

Salima, M., Youcef, M., Bouarroudj, T., Chetoui, A., Belkhettab, I., Bezzi, H., Aoudjit, L., Zioui, D., Ziouche, A. & Mekki, D. 2023 Sunlight-assisted photocatalytic degradation of tartrazine in the presence of Mg doped ZnS nanocatalysts. *Solid State Sciences* **143**, 107260. https://doi.org/10.1016/j.solidstatesciences.2023.107260.

Saoud, W. A., Belkessa, N., Azzaz, A. A., Rochas, V., Mezino, V., Presset, M.-A., Lechevin, S., Genouel, A., Rouxel, S., Monsimert, D., Bouzaza, A., Gloux, A., Cantin, D. & Assadi, A. A. 2023 Pilot scale investigation of DBD-Plasma photocatalysis for industrial application in livestock building air: Elimination of chemical pollutants and odors. *Chemical Engineering Journal* **468**, 143710. https://doi.org/10.1016/j.cej.2023.143710.

Sarker, B., Keya, N., I, K., Mahir, F., Nahiun, M., Shahida, K., & A, S. & Khan, R. 2021 Surface and ground water pollution: Causes and effects of urbanization and industrialization in South Asia. *Scientific Review* **73**, 32–41. https://doi.org/10.32861/sr.73.32.41.

Sharma, A., Makhija, A., Dahiya, S., Ohlan, A., Punia, R. & Maan, A. S. 2023 Rietveld refinement, morphological, optical and photocatalytic dye degradation studies of pristine and Sr-doped SnS2 hexagonal nanoplates. *Materials Research Bulletin* 112464. https://doi.org/10.1016/j.materresbull.2023.112464.

Shen, J., Yuan, Y., Duan, F. & Li, Y. 2023 Performance of resin adsorption and ozonation pretreatment in mitigating organic fouling of reverse osmosis membrane. *Journal of Water Process Engineering* **53**, 103688. https://doi.org/10.1016/j.jwpe.2023.103688.

Sun, X., He, K., Chen, Z., Yuan, H., Guo, F. & Shi, W. 2023 Construction of visible-light-response photocatalysis-self-Fenton system for the efficient degradation of amoxicillin based on industrial waste red mud/CdS S-scheme heterojunction. *Separation and Purification Technology* **324**, 124600. https://doi.org/10.1016/j.seppur.2023.124600.

Tian, M., He, X., Feng, Y., Wang, W., Chen, H., Gong, M., Liu, D., Clarke, J. L. & van Eerde, A. 2021 Pollution by antibiotics and antimicrobial resistance in liveStock and poultry manure in China, and countermeasures. *Antibiotics* **10** (5), 539. https://doi.org/10.3390/antibiotics10050539.

Tian, H., Liu, J., Zhang, Y. & Yue, P. 2023 A novel integrated industrial-scale biological reactor for odor control in a sewage sludge composting facility: Performance, pollutant transformation, and bioaerosol emission mechanism. *Waste Management* **164**, 9–19. https://doi.org/10.1016/j.wasman.2023.03.021.

Tran, T. H., Phi, T. H., Nguyen, H. N., Pham, N. H., Nguyen, C. V., Ho, K. H., Doan, Q. K., Le, V. Q., Nguyen, T. T. & Nguyen, V. T. 2020 Sr doped lamno3 nanoparticles prepared by microwave combustion method: A recyclable visible light photocatalyst. *Results in Physics* **19**, 103417. https://doi.org/10.1016/j.rinp.2020.103417.

Uma, H. B., Kumar, M. S. V. & Ananda, S. 2022 Semiconductor-assisted photodegradation of textile dye, photo-voltaic and antibacterial property of electrochemically synthesized Sr-doped CuO nano photocatalysts. *Journal of Molecular Structure* **1264**, 133110. https://doi.org/10.1016/j.molstruc.2022.133110.

Vaughn, D. D., Hentz, O. D., Chen, S., Wang, D. & Schaak, R. E. 2012 Formation of SnS nanoflowers for lithium ion batteries. *Chemical Communications* **48** (45), 5608. https://doi.org/10.1039/c2cc32033a.

Wang, H., Zhang, G. & Gao, Y. 2010 Photocatalytic degradation of metronidazole in aqueous solution by niobate k6nb10.8o30. *Wuhan University Journal of Natural Sciences* **15** (4), 345–349. https://doi.org/10.1007/s11859-010-0664-0.

Wang, B., Li, X. & Wang, Y. 2022a Degradation of metronidazole in water using dielectric barrier discharge synergistic with sodium persulfate. *Separation and Purification Technology* **303**, 122173. https://doi.org/10.1016/j.seppur.2022.122173.

Wang, P., Xu, C., Zhang, X., Yuan, Q. & Shan, S. 2023a Effect of photocatalysis on the physicochemical properties of liquid digestate. *Environmental Research* **223**, 115467. https://doi.org/10.1016/j.envres.2023.115467.

Wardighi, Z., El Amri, A., Kadiri, L., Jebli, A., Bouhassane, F. Z., Rifi, E. H. & Lebkiri, A. 2023 Ecological study of elimination of the organic pollutant (violet crystal) using natural fibers of Rubia tinctorum: Optimization of adsorption processes by BBD-RSM modeling and DFT approaches. *Inorganic Chemistry Communications* **155**, 111014. https://doi.org/10.1016/j.inoche.2023.111014.

Weldeslassie, T., Naz, H., Singh, B., Oves, M., 2018 Chemical Contaminants for Soil, Air and Aquatic Ecosystem. In: *Modern Age Environmental Problems and Their Remediation* (Oves, M., Zain Khan, M. & M.I. Ismail, I. eds.). Springer International Publishing, Cham, Switzerland, pp. 1–22.

Wu, C., Liu, X., Wei, D., Fan, J. & Wang, L. 2001 Photosonochemical degradation of Phenol in water. *Water Research* **35** (16), 3927–3933. https://doi.org/10.1016/S0043-1354(01)00133-6.

Yang, L., Zhou, Y., Chen, L., Chen, H., Liu, W., Zheng, W., Andersen, M. E., Zhang, Y., Hu, Y., Crabbe, M. J. C. & Qu, W. 2022 Single enrichment systems possibly underestimate both exposures and biological effects of organic pollutants from drinking water. *Chemosphere* **292**, 133496. https://doi.org/10.1016/j.chemosphere.2021.133496.

Yang, H., Xu, L., Li, Y., Liu, H., Wu, X., Zhou, P., Graham, N. J. D. & Yu, W. 2023 Fexo/FeNC modified activated carbon packing media for biological slow filtration to enhance the removal of dissolved organic matter in reused water. *Journal of Hazardous Materials* **457**, 131736. https://doi.org/10.1016/j.jhazmat.2023.131736.

Yarahmadi, M., Maleki-Ghaleh, H., Mehr, M. E., Dargahi, Z., Rasouli, F. & Siadati, M. H. 2021 Synthesis and characterization of Sr-doped ZnO nanoparticles for photocatalytic applications. *Journal of Alloys and Compounds* **853**, 157000. https://doi.org/10.1016/j.jallcom.2020.157000.

Yin, K., Yan, Z., Fang, N., Yu, W., Chu, Y., Shu, S. & Xu, M. 2023 The synergistic effect of surface vacancies and heterojunctions for efficient photocatalysis: A review. *Separation and Purification Technology* **325**, 124636. https://doi.org/10.1016/j.seppur.2023.124636.

Yu, D., Bai, J., Liang, H. & Li, C. 2016 Electrospinning, solvothermal, and self-assembly synthesis of recyclable and renewable AgBr TiO2/CNFs with excellent visible-light responsive photocatalysis. *Journal of Alloys and Compounds* **683**, 329–338. https://doi.org/10.1016/j.jallcom.2016.05.103.

Yu, R., Yang, Y., Zhou, Z., Li, X., Liu, C. & Sun, T. 2023 Role of visible light photocatalysis in alleviation and mechanism transformation of ultrafiltration membrane fouling caused by natural organic matter. *Separation and Purification Technology* **324**, 124409. https://doi.org/10.1016/j.seppur.2023.124409.

Zhang, R., Cai, L., Cai, Y., Han, Q., Li, Y., Zhang, T., Liu, Y., Zeng, K., Zhao, C., Yu, J. & Yang, Z. 2021 Lamellar insert SnS2 anchored on BiOBr for enhanced photocatalytic degradation of organic pollutant under visible-light. *Colloids and Surfaces A: Physicochemical and Engineering Aspects* **618**, 126444. https://doi.org/10.1016/j.colsurfa.2021.126444.

Zhang, T., Wang, P., Li, Y., Bao, Y., Lim, T.-T. & Zhan, S. 2023 Advances in dual-functional photocatalysis for simultaneous reduction of hexavalent chromium and oxidation of organics in wastewater. *Environmental Functional Materials* S2773058123000182. https://doi.org/10.1016/j.efmat.2023.05.001.

Zhao, D., Zhou, Y., Deng, Y., Xiang, Y., Zhang, Y., Zhao, Z. & Zeng, D. 2018 A novel and reusable RGO/ZnO with nanosheets/Microparticle composite photocatalysts for efficient pollutants degradation. *ChemistrySelect* **3** (30), 8740–8747. https://doi.org/10.1002/slct.201801609.

Zioui, D., Salazar, H., Aoudjit, L., Martins, P. M. & Lanceros-Méndez, S. 2019 Polymer-based membranes for oily wastewater remediation. *Polymers* **12** (1), 42. https://doi.org/10.3390/polym12010042.

Zioui, D., Aoudjit. L., Touahra, F. & Bachari, K. 2022 Preparation and characterization of TiO2 - chitosan composite films and application for tartrazine dye degradation. *Cellulose Chem. Technol.* **56**, 1101, https://doi.org/10.35812/CelluloseChemTechnol.2022.56.98.

Zioui, D., Martins, P. M., Aoudjit, L., Salazar, H. & Lanceros-Méndez, S. 2023 Wastewater treatment of real effluents by microfiltration using poly(vinylidene fluoride–hexafluoropropylene) membranes. *Polymers* **15** (5), 1143. https://doi.org/10.3390/polym15051143.

First received 13 August 2023; accepted in revised form 3 February 2024. Available online 23 February 2024